Research Article | Vol. 25, No. 13 | 26 Jun 2017 | OPTICS EXPRESS 14192
Optics EXPRESS

Sub-cycle steering of the deprotonation of acetylene by intense few-cycle mid-infrared laser fields

H. Li,[1,2] Nora G. Kling,[2] T. Gaumnitz,[3] C. Burger,[2,4] R. Siemering,[5] J. Schötz,[2,4] Q. Liu,[2,4] L. Ban,[3] Y. Pertot,[3] J. Wu,[1] A. M. Azzeer,[6] R. de Vivie-Riedle,[5] H. J. Wörner,[3] and M. F. Kling[2,4,*]

[1]*State Key Laboratory of Precision Spectroscopy, East China Normal University, Shanghai 200062, China*
[2]*Department of Physics, Ludwig-Maximilians-Universität Munich, D-85748 Garching, Germany*
[3]*Laboratorium für Physikalische Chemie, ETH Zürich, 8093 Zürich, Switzerland*
[4]*Max Planck Institute of Quantum Optics, D-85748 Garching, Germany*
[5]*Department of Chemistry and Biochemistry, Ludwig-Maximilians-Universität Munich, D-81377 München, Germany*
[6]*Department of Physics & Astronomy, King-Saud University, Riyadh 11451, Saudi Arabia*
[*]*matthias.kling@lmu.de*

Abstract: Directional breaking of the C-H/C-D molecular bond is manipulated in acetylene (C_2H_2) and deuterated acetylene (C_2D_2) by waveform controlled few-cycle mid-infrared laser pulses with a central wavelength around 1.6 μm at an intensity of about 8×10^{13} W/cm^2. The directionality of the deprotonation of acetylene is controlled by changing the carrier-envelope phase (CEP). The CEP-control can be attributed to the laser-induced superposition of vibrational modes, which is sensitive to the sub-cycle evolution of the laser waveform. Our experiments and simulations indicate that near-resonant, intense mid-infrared pulses permit a higher degree of control of the directionality of the reaction compared to those obtained in near-infrared fields, in particular for the deuterated species.

OCIS codes: (020.0020) Atomic and molecular physics; (020.2649) Strong field laser physics; (320.7120) Ultrafast phenomena.

References and links

1. X. Xie, K. Doblhoff-Dier, S. Roither, M. S. Schöffler, D. Kartashov, H. Xu, T. Rathje, G. G. Paulus, A. Baltuška, S. Gräfe, and M. Kitzler, "Attosecond-Recollision-Controlled Selective Fragmentation of Polyatomic Molecules," Phys. Rev. Lett. **109**(24), 243001 (2012).
2. H. Xu, C. Marceau, K. Nakai, T. Okino, S.-L. Chin, and K. Yamanouchi, "Communication: Two stages of ultrafast hydrogen migration in methanol driven by intense laser fields," J. Chem. Phys. **133**(7), 071103 (2010).
3. H. Xu, T. Okino, and K. Yamanouchi, "Tracing ultrafast hydrogen migration in allene in intense laser fields by triple-ion coincidence momentum imaging," J. Chem. Phys. **131**(15), 151102 (2009).
4. H. Xu, T. Okino, and K. Yamanouchi, "Ultrafast hydrogen migration in allene in intense laser fields: Evidence of two-body Coulomb explosion," Chem. Phys. Lett. **469**(4-6), 255–260 (2009).
5. H. Xu, T. Okino, T. Kudou, K. Yamanouchi, S. Roither, M. Kitzler, A. Baltuska, and S.-L. Chin, "Effect of Laser Parameters on Ultrafast Hydrogen Migration in Methanol Studied by Coincidence Momentum Imaging," J. Phys. Chem. A **116**(11), 2686–2690 (2012).
6. S. Miura, T. Ando, K. Ootaka, A. Iwasaki, H. Xu, T. Okino, K. Yamanouchi, D. Hoff, T. Rathje, G. G. Paulus, M. Kitzler, A. Baltuška, G. Sansone, and M. Nisoli, "Carrier-envelope-phase dependence of asymmetric CD bond breaking in C_2D_2 in an intense few-cycle laser field," Chem. Phys. Lett. **595–596**, 61–66 (2014).
7. K. Hoshina, Y. Furukawa, T. Okino, and K. Yamanouchi, "Efficient ejection of H_3^+ from hydrocarbon molecules induced by ultrashort intense laser fields," J. Chem. Phys. **129**(10), 104302 (2008).
8. S. Kaziannis, I. Liontos, G. Karras, C. Corsi, M. Bellini, and C. Kosmidis, "The ejection of triatomic molecular hydrogen ions H_3^+ produced by the interaction of benzene molecules with ultrafast laser pulses," J. Chem. Phys. **131**(14), 144308 (2009).
9. A. Hishikawa, A. Matsuda, M. Fushitani, and E. J. Takahashi, "Visualizing Recurrently Migrating Hydrogen in Acetylene Dication by Intense Ultrashort Laser Pulses," Phys. Rev. Lett. **99**(25), 258302 (2007).

#292815 https://doi.org/10.1364/OE.25.014192
Journal © 2017 Received 14 Apr 2017; revised 2 Jun 2017; accepted 2 Jun 2017; published 13 Jun 2017

Optics EXPRESS

10. H. Xu, T. Okino, K. Nakai, K. Yamanouchi, S. Roither, X. Xie, D. Kartashov, L. Zhang, A. Baltuska, and M. Kitzler, "Two-proton migration in 1,3-butadiene in intense laser fields," Phys. Chem. Chem. Phys. **12**(40), 12939–12942 (2010).
11. T. Okino, A. Watanabe, H. Xu, and K. Yamanouchi, "Ultrafast hydrogen scrambling in methylacetylene and methyl-d3-acetylene ions induced by intense laser fields," Phys. Chem. Chem. Phys. **14**(30), 10640–10646 (2012).
12. E. Wells, C. E. Rallis, M. Zohrabi, R. Siemering, B. Jochim, P. R. Andrews, U. Ablikim, B. Gaire, S. De, K. D. Carnes, B. Bergues, R. de Vivie-Riedle, M. F. Kling, and I. Ben-Itzhak, "Adaptive strong-field control of chemical dynamics guided by three-dimensional momentum imaging," Nat. Commun. **4**, 2895 (2013).
13. M. Kübel, R. Siemering, C. Burger, N. G. Kling, H. Li, A. S. Alnaser, B. Bergues, S. Zherebtsov, A. M. Azzeer, I. Ben-Itzhak, R. Moshammer, R. de Vivie-Riedle, and M. F. Kling, "Steering Proton Migration in Hydrocarbons Using Intense Few-Cycle Laser Fields," Phys. Rev. Lett. **116**(19), 193001 (2016).
14. A. S. Alnaser, M. Kübel, R. Siemering, B. Bergues, N. G. Kling, K. J. Betsch, Y. Deng, J. Schmidt, Z. A. Alahmed, A. M. Azzeer, J. Ullrich, I. Ben-Itzhak, R. Moshammer, U. Kleineberg, F. Krausz, R. de Vivie-Riedle, and M. F. Kling, "Subfemtosecond steering of hydrocarbon deprotonation through superposition of vibrational modes," Nat. Commun. **5**, 3800 (2014).
15. H. Li, N. G. Kling, B. Förg, J. Stierle, A. Kessel, S. A. Trushin, M. F. Kling, and S. Kaziannis, "Carrier-envelope phase dependence of the directional fragmentation and hydrogen migration in toluene in few-cycle laser fields," Struct. Dyn. **3**(4), 043206 (2016).
16. C. Burger, N. G. Kling, R. Siemering, A. S. Alnaser, B. Bergues, A. M. Azzeer, R. Moshammer, R. de Vivie-Riedle, M. Kübel, and M. F. Kling, "Visualization of bond rearrangements in acetylene using near single-cycle laser pulses," Faraday Discuss. **194**, 495–508 (2016).
17. N. Schirmel, N. Reusch, P. Horsch, and K.-M. Weitzel, "Formation of fragment ions (H^+, H_3^+, CH_3^+) from ethane in intense femtosecond laser fields - from understanding to control," Faraday Discuss. **163**, 461–474, discussion 513–543 (2013).
18. M. F. Kling, Ch. Siedschlag, A. J. Verhoef, J. I. Khan, M. Schultze, T. Uphues, Y. Ni, M. Uiberacker, M. Drescher, F. Krausz, and M. J. J. Vrakking, "Control of Electron Localization in Molecular Dissociation," Science **312**(5771), 246–248 (2006).
19. H. Li, A. S. Alnaser, X. M. Tong, K. J. Betsch, M. Kübel, T. Pischke, B. Förg, J. Schötz, F. Süßmann, S. Zherebtsov, B. Bergues, A. Kessel, S. A. Trushin, A. M. Azzeer, and M. F. Kling, "Intensity dependence of the attosecond control of the dissociative ionization of D_2," J. Phys. At. Mol. Opt. Phys. **47**(12), 124020 (2014).
20. I. Znakovskaya, P. von den Hoff, G. Marcus, S. Zherebtsov, B. Bergues, X. Gu, Y. Deng, M. J. J. Vrakking, R. Kienberger, F. Krausz, R. de Vivie-Riedle, and M. F. Kling, "Subcycle Controlled Charge-Directed Reactivity with Few-Cycle Midinfrared Pulses," Phys. Rev. Lett. **108**(6), 063002 (2012).
21. X. Han, J. P. Maclean, D. E. Laban, W. C. Wallace, D. Kielpinski, R. T. Sang, and I. V. Litvinyuk, "Carrier-envelope-phase-dependent dissociation of hydrogen," New J. Phys. **15**(2), 023034 (2013).
22. D. Ray, F. He, S. De, W. Cao, H. Mashiko, P. Ranitovic, K. P. Singh, I. Znakovskaya, U. Thumm, G. G. Paulus, M. F. Kling, I. V. Litvinyuk, and C. L. Cocke, "Ion-Energy Dependence of Asymmetric Dissociation of D_2 by a Two-Color Laser Field," Phys. Rev. Lett. **103**(22), 223201 (2009).
23. H. Xu, H. Hu, X.-M. Tong, P. Liu, R. Li, R. T. Sang, and I. V. Litvinyuk, "Coherent control of the dissociation probability of H_2^+ in ω-3ω two-color fields," Phys. Rev. A **93**(6), 063416 (2016).
24. J. Wu, A. Vredenborg, L. P. H. Schmidt, T. Jahnke, A. Czasch, and R. Dörner, "Comparison of dissociative ionization of H_2, N_2, Ar_2, and CO by elliptically polarized two-color pulses," Phys. Rev. A **87**(2), 023406 (2013).
25. Q. Song, X. Gong, Q. Ji, K. Lin, H. Pan, J. Ding, H. Zeng, and J. Wu, "Directional deprotonation ionization of acetylene in asymmetric two-color laser fields," J. Phys. At. Mol. Opt. Phys. **48**(9), 094007 (2015).
26. K. Liu, Q. Zhang, and P. Lu, "Enhancing electron localization in molecular dissociation by two-color mid- and near-infrared laser fields," Phys. Rev. A **86**(3), 033410 (2012).
27. M. Kübel, C. Burger, R. Siemering, N. G. Kling, B. Bergues, A. S. Alnaser, I. Ben-Itzhak, R. Moshammer, R. de Vivie-Riedle, and M. F. Kling, "Phase- and intensity-dependence of ultrafast dynamics in hydrocarbon molecules in few-cycle laser fields," Mol. Phys. (2017).
28. H. Li, X. M. Tong, N. Schirmel, G. Urbasch, K. J. Betsch, S. Zherebtsov, F. Süßmann, A. Kessel, S. A. Trushin, G. G. Paulus, K. M. Weitzel, and M. F. Kling, "Intensity dependence of the dissociative ionization of DCl in few-cycle laser fields," J. Phys. At. Mol. Opt. Phys. **49**(1), 015601 (2016).
29. H. Li, B. Mignolet, G. Wachter, S. Skruszewicz, S. Zherebtsov, F. Süssmann, A. Kessel, S. A. Trushin, N. G. Kling, M. Kübel, B. Ahn, D. Kim, I. Ben-Itzhak, C. L. Cocke, T. Fennel, J. Tiggesbäumker, K. H. Meiwes-Broer, C. Lemell, J. Burgdörfer, R. D. Levine, F. Remacle, and M. F. Kling, "Coherent Electronic Wave Packet Motion in C_{60} Controlled by the Waveform and Polarization of Few-Cycle Laser Fields," Phys. Rev. Lett. **114**(12), 123004 (2015).
30. M. Krüger, M. Schenk, and P. Hommelhoff, "Attosecond control of electrons emitted from a nanoscale metal tip," Nature **475**(7354), 78–81 (2011).
31. S. Zherebtsov, T. Fennel, J. Plenge, E. Antonsson, I. Znakovskaya, A. Wirth, O. Herrwerth, F. Suszmann, C. Peltz, I. Ahmad, S. A. Trushin, V. Pervak, S. Karsch, M. J. J. Vrakking, B. Langer, C. Graf, M. I. Stockman, F. Krausz, E. Ruhl, and M. F. Kling, "Controlled near-field enhanced electron acceleration from dielectric nanospheres with intense few-cycle laser fields," Nat. Phys. **7**(8), 656–662 (2011).

Optics EXPRESS

32. S. Zherebtsov, F. Süßmann, C. Peltz, J. Plenge, K. J. Betsch, I. Znakovskaya, A. S. Alnaser, N. G. Johnson, M. Kübel, A. Horn, V. Mondes, C. Graf, S. A. Trushin, A. Azzeer, M. J. J. Vrakking, G. G. Paulus, F. Krausz, E. Rühl, T. Fennel, and M. F. Kling, "Carrier–envelope phase-tagged imaging of the controlled electron acceleration from SiO_2 nanospheres in intense few-cycle laser fields," New J. Phys. **14**(7), 075010 (2012).
33. F. Süssmann, S. Zherebtsov, J. Plenge, N. G. Johnson, M. Kübel, A. M. Sayler, V. Mondes, C. Graf, E. Rühl, G. G. Paulus, D. Schmischke, P. Swrschek, and M. F. Kling, "Single-shot velocity-map imaging of attosecond light-field control at kilohertz rate," Rev. Sci. Instrum. **82**(9), 093109 (2011).
34. T. Rathje, G. J. Nora, M. Möller, F. Süßmann, D. Adolph, M. Kübel, R. Kienberger, M. F. Kling, G. G. Paulus, and A. M. Sayler, "Review of attosecond resolved measurement and control via carrier–envelope phase tagging with above-threshold ionization," J. Phys. At. Mol. Opt. Phys. **45**(7), 074003 (2012).
35. N. G. Johnson, O. Herrwerth, A. Wirth, S. De, I. Ben-Itzhak, M. Lezius, B. Bergues, M. F. Kling, A. Senftleben, C. D. Schröter, R. Moshammer, J. Ullrich, K. J. Betsch, R. R. Jones, A. M. Sayler, T. Rathje, K. Rühle, W. Müller, and G. G. Paulus, "Single-shot carrier-envelope-phase-tagged ion-momentum imaging of nonsequential double ionization of argon in intense 4-fs laser fields," Phys. Rev. A **83**(1), 013412 (2011).
36. P. Colosimo, G. Doumy, C. I. Blaga, J. Wheeler, C. Hauri, F. Catoire, J. Tate, R. Chirla, A. M. March, G. G. Paulus, H. G. Muller, P. Agostini, and L. F. DiMauro, "Scaling strong-field interactions towards the classical limit," Nat. Phys. **4**(5), 386–389 (2008).
37. P. Agostini and L. F. DiMauro, "Chapter 3 - Atomic and Molecular Ionization Dynamics in Strong Laser Fields: From Optical to X-rays," in *Advances In Atomic, Molecular, and Optical Physics*, E. A. Paul Berman and L. Chun, eds. (Academic Press, 2012), pp. 117–158.
38. R. R. Goruganthu and W. G. Wilson, "Relative electron detection efficiency of microchannel plates from 0–3 keV," Rev. Sci. Instrum. **55**(12), 2030–2033 (1984).
39. B. Bergues, S. Zherebtsov, Y. Deng, X. Gu, I. Znakovskaya, R. Kienberger, F. Krausz, G. Marcus, and M. F. Kling, "Sub-cycle electron control in the photoionization of xenon using a few-cycle laser pulse in the mid-infrared," New J. Phys. **13**(6), 063010 (2011).
40. M. J. J. Vrakking, "An iterative procedure for the inversion of two-dimensional ion/photoelectron imaging experiments," Rev. Sci. Instrum. **72**(11), 4084–4089 (2001).
41. H. J. Werner, P. J. Knowles, and G. Knizia, "A Package of Ab-Initio Programs," MolPro (2006).
42. K. Yamanouchi, "The Next Frontier," Science **295**(5560), 1659–1660 (2002).
43. A. D. Bandrauk, W. S. Sedik, and C. F. Matta, "Effect of absolute laser phase on reaction paths in laser-induced chemical reactions," J. Chem. Phys. **121**(16), 7764–7775 (2004).
44. A. N. Markevitch, D. A. Romanov, S. M. Smith, and R. J. Levis, "Rapid Proton Transfer Mediated by a Strong Laser Field," Phys. Rev. Lett. **96**(16), 163002 (2006).
45. X. Gong, Q. Song, Q. Ji, H. Pan, J. Ding, J. Wu, and H. Zeng, "Strong-Field Dissociative Double Ionization of Acetylene," Phys. Rev. Lett. **112**(24), 243001 (2014).
46. X. Xie, K. Doblhoff-Dier, H. Xu, S. Roither, M. S. Schöffler, D. Kartashov, S. Erattupuzha, T. Rathje, G. G. Paulus, K. Yamanouchi, A. Baltuška, S. Gräfe, and M. Kitzler, "Selective Control over Fragmentation Reactions in Polyatomic Molecules Using Impulsive Laser Alignment," Phys. Rev. Lett. **112**(16), 163003 (2014).
47. T. Zuo and A. D. Bandrauk, "Charge-resonance-enhanced ionization of diatomic molecular ions by intense lasers," Phys. Rev. A **52**(4), R2511–R2514 (1995).
48. X. Xie, S. Roither, M. Schöffler, H. Xu, S. Bubin, E. Lötstedt, S. Erattuphuza, A. Iwasaki, D. Kartashov, K. Varga, G. G. Paulus, A. Baltuška, K. Yamanouchi, and M. Kitzler, "Role of proton dynamics in efficient photoionization of hydrocarbon molecules," Phys. Rev. A **89**, 023429 (2014).
49. S. Roither, X. Xie, D. Kartashov, L. Zhang, M. Schöffler, H. Xu, A. Iwasaki, T. Okino, K. Yamanouchi, A. Baltuska, and M. Kitzler, "High Energy Proton Ejection from Hydrocarbon Molecules Driven by highly Efficient Field Ionization," Phys. Rev. Lett. **106**(16), 163001 (2011).
50. K. Liu, Q. Zhang, P. Lan, and P. Lu, "Anomalous isotopic effect on electron-directed reactivity by a 3-μm midinfrared pulse," Opt. Express **21**(4), 5107–5116 (2013).

1. Introduction

Controlling molecular structure rearrangements using ultrashort laser fields has attracted enormous interest for the last decades [1–17]. Chemical transformations can be controlled with various laser parameters, including intensity, pulse duration, chirp, and the electric field waveform. The latter has been introduced to control the directionality of a molecular process for symmetric molecules. A classic example is the dissociative ionization of neutral molecular hydrogen into a hydrogen atom and a proton, where the field controls the emission direction of the two fragments. This control has been achieved with tailored waveforms resulting from either carrier-envelope phase (CEP) controlled few-cycle pulses [18–21] or synthesized femtosecond laser fields composed of at least two different colors, e.g. in ω-2ω fields [22–26]. The underlying mechanism is based on the coherent superposition of electronic states with different parity and importantly, goes beyond the Born-Oppenheimer approximation. So far, the control with laser fields with tailored waveforms has mostly concentrated on the

Optics EXPRESS

dissociative ionization of diatomic molecules, and the theoretical modeling using semi-classical and quantum mechanical calculations. Advances in theory have brought more complex targets into the focus of recent and current research efforts, including polyatomic molecules [6, 13–16, 27, 28], fullerenes [29], and nanostructures [30–32].

The control of reactions occurring in hydrocarbon molecules is interesting from both a fundamental and an application point of view. The processes that may be steered with tailored fields include C-H and C-C bond breaking and proton migration reactions [4, 6, 13–16]. A prototype system is acetylene, where it was demonstrated that both the directionality of the deprotonation [6, 14] and proton migration [13] can be steered with the CEP of few-cycle pulses in the visible to near-infrared (NIR) region. Recent studies suggested that the directional control over these reactions in hydrocarbon molecules follows a different scheme, where the laser field coherently couples vibrational degrees of freedom.

With the advent of intense few-cycle laser systems in the mid-infrared (MIR), the control over molecular processes can be extended into this wavelength regime. This regime is particularly appealing for studying molecules, where the vibrational modes can be excited resonantly. Resonant excitation is expected to lead to a higher degree of control. Despite the benefits of using longer wavelength lasers to control molecular reactions, so far experimental studies have been limited to the dissociative ionization of hydrogen [20]. In our present work, we carried out a joint experimental and theoretical study on the CEP-control of the deprotonation direction of acetylene and deuterated acetylene in intense, few-cycle MIR laser fields.

2. Experimental setup

The CEP-dependence of the directionality of the H/D ion emission from C_2H_2/C_2D_2 induced by intense few-cycle MIR pulses is investigated using a phase-tagged single-shot velocity map imaging (VMI) setup [33]. A beam of linearly polarized NIR pulses centered at 790 nm with a pulse duration of about 30 fs (FEMTOPOWER PRO V CEP by Femtolasers at ETH Zürich) is frequency transformed to the MIR wavelength region in an optical parametric amplifier (HE-TOPAS). The linearly polarized MIR pulses are then spectrally broadened in a gas-filled hollow-core fiber, and compressed in time by passing through bulk fused silica. The resulting few-cycle pulses have a central wavelength of about 1.6 μm. The pulse duration is estimated to be around 2 optical cycles (one optical cycle is about 5.3 fs) from a frequency-resolved optical gating (FROG) measurement. The relative CEP of the broadband MIR laser pulses was measured using a single-shot stereographic above-threshold-ionization phase meter ('phase meter' for short) [34]. Simultaneous measurement of the CEP and the acetylene fragments in the VMI on a shot-by-shot basis allows for "tagging" each laser shot with its relative CEP, shown schematically in Fig. 1. As the process of generating the MIR pulses is intrinsically CEP-locked, the CEP was scanned by insertion of fused silica into the beam path common to both devices. Scanning through the 0 to 2π phase range a few times per minute ensures that the accumulated CEP over the duration of the scan (several hours) is sufficiently random. The measured angle theta is converted to CEP values following a previously reported procedure [35].

Optics EXPRESS

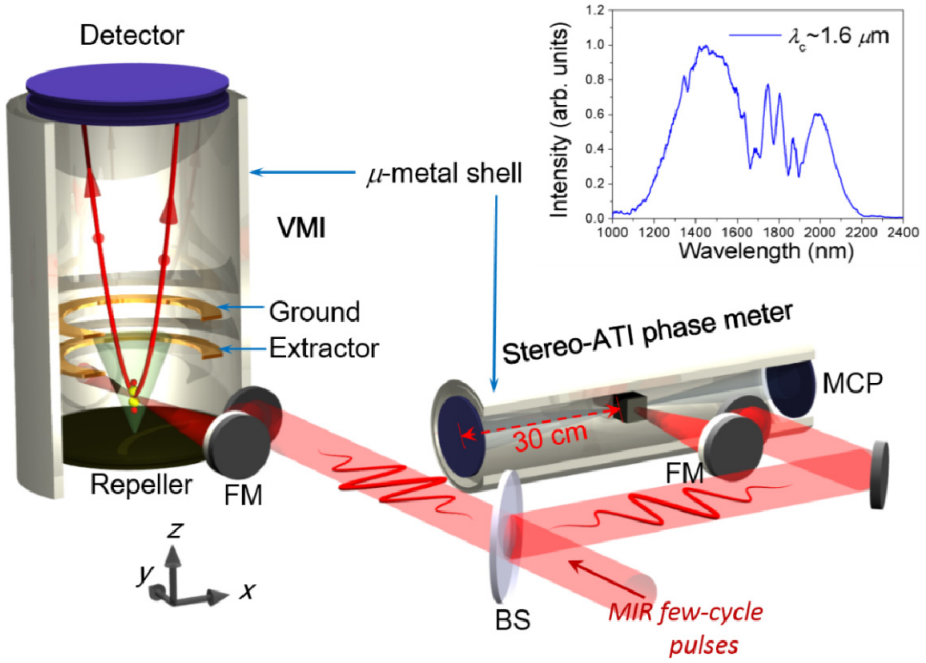

Fig. 1. Schematic depiction of the single-shot phase-tagged VMI experimental apparatus. FM stands for focusing mirror and BS stands for beam splitter. The inserted plot on the upper right corner is the spectrum for the few-cycle MIR pulse. The central wavelength is around 1.6 μm.

As shown in Fig. 1, the phase meter for the MIR spectral range is similar to the phase meter designed for pulses with wavelengths centered around 700-800 nm [34]. The pulses are focused into a gas cell containing ~10^{-2} torr of xenon gas. Two small slits (2 mm wide, 1 mm high) allow for electrons generated in the laser focus to travel out of the cell and towards the detectors, microchannel plates (MCPs) with metal anodes (Photonis, model 31373), situated along the axis of the laser polarization. A μ-metal tube, concentric with the flight-tubes, shields the electrons from stray magnetic fields. As the recollision energy for a laser intensity of 8×10^{13} W/cm^2 at 1.6 μm is much higher (U_p ~19 eV, where U_p is the ponderomotive potential and is defined by $U_p = I/(4\omega^2)$ in atomic units) compared to the NIR wavelengths (U_p (800 nm) ~5 eV), the energy of the electrons from the back-scattered part of the spectrum is also much higher. To account for this, the length of flight tubes was increased to 30 cm (the flight tubes are 17.5 cm long for the NIR phase meter) such that the time of flight for these higher energy electrons has a resolution of about 1 ns. Interestingly, the number of electrons detected per laser shot is about a fourth of that detected for the NIR phase meter. The reduced count rate is greatly attributed to the fact that the number of re-scattered electrons is drastically reduced with increasing wavelength [36, 37]. Furthermore, the half-angle for the detected cone of electrons is only 2.5°, compared to 4.3° for the NIR phase meter. Lastly, the detector efficiency is lower for the higher energy electrons [38]. The fact that the re-scattered electron count rate is still sufficient is likely due to the target not being depleted [39].

The transmission of the MIR laser through the beam splitter is focused into the interaction region of the VMI spectrometer. The pulses intersect a diffusive molecular beam originating from a 100 μm diameter hole at the center of the repeller plate. The laser intensity is estimated by measuring the kinetic energy spectra of the ATI electron emission from Xe under identical experimental conditions [19, 29]. H/D ions generated in the VMI focus during laser-molecule interactions are imaged onto a complementary metal-oxide-semiconductor (CMOS) camera. For each laser shot, a VMI image is detected together with a CEP value obtained from the phase meter. There is an inherent constant phase offset between the phase meter and the VMI

Optics EXPRESS

spectrometer. Thus, the absolute phase is determined by comparison with a reference data set where we measure electrons from the single ionization of Xe [19, 29]. In the post-processing steps, the whole branch of VMI images obtained from every laser shot is sorted and binned into 20 images for CEPs ranging from 0 to 2π. Then Abel-inversion [40] is applied to the resulting images to extract the 2D momentum distributions around the plane of $p_z = 0$ from the 3D distributions.

3. Theoretical model

A quantum dynamical model is applied to explain the deprotonation mechanism. The model was previously developed to investigate deprotonation and hydrogen migration in small hydrocarbons ionized by NIR few-cycle laser fields [13, 14]. In this work, it is extended to the MIR spectral region. The program package MOLPRO [41] was utilized to perform *ab initio* calculations for the potential energy surfaces (PESs) of C_2H_2 and C_2D_2 and the corresponding dipole and transition dipole moments. The method was CASSCF(10,10) for the ground and excited states of the neutral molecule, CASSCF(9,10) for the ground and excited states of the cation and CASSCF(8,10) for the ground and excited states of the dication with the 6-311 + + G** basis set and a step size along the two normal modes of 0.05 au. Figure 2 shows the symmetric and anti-symmetric stretching coordinates [Fig. 2(a)] and the 2D PES of the excited dicationic state $A^3\Pi_u$ [Fig. 2(b)]. The PES were interpolated to 256 × 256 points for the potential Hamilton operator in the nuclear wave packet calculations.

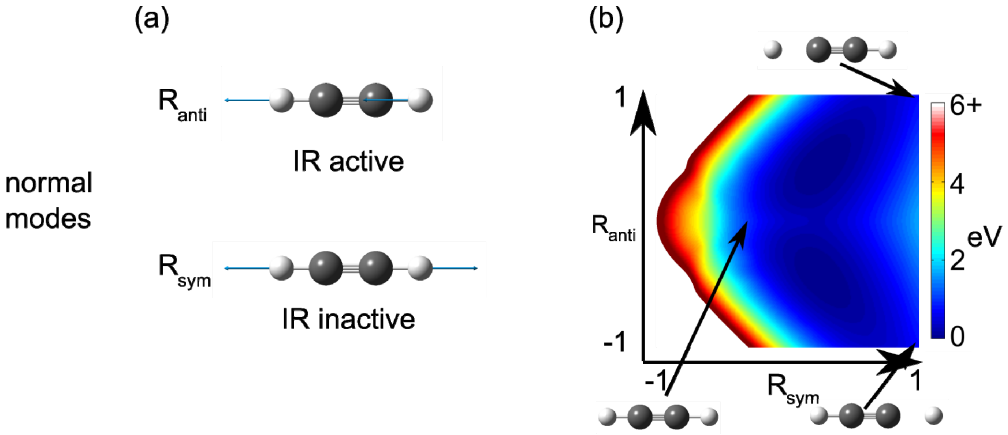

Fig. 2. (a) Normal modes used for the theoretical description of the deprotonation of acetylene. (b) 2D PES of the excited dicationic state $A^3\Pi_u$.

The time-dependent Schrödinger equation (TDSE) is solved numerically using the Chebychev propagator and time steps of 0.024 fs. With H_n as the Hamiltonian of the $X^1\Sigma_g^+$ state, μ_{nn} as the associated dipole moment, and $\varepsilon(t)$ as the representation of the laser field for the MIR pulses, the TDSE for the nuclear wave function $\Psi_n(t)$ of neutral C_2H_2/C_2D_2 molecules in the light field is written as

$$\left(H_n + \mu_{nn}\varepsilon(t)\right)\Psi_n(t) = \tilde{\Psi}_n(t). \tag{1}$$

The laser field at angular frequency ω, with CEP φ, a full width at half maximum FWHM and a cycle-averaged intensity I of 8×10^{13} W/cm^2 can be written as

$$\varepsilon(t) = \sqrt{I}\,exp\left[-\left(\frac{t}{FWHM/\sqrt{2ln2}}\right)^2\right]cos(\omega t - \varphi). \tag{2}$$

Optics EXPRESS

The calculation were performed with different laser parameters. The CEP was varied in steps of 0.1 π and the wavelength $\lambda = \frac{2\pi}{\omega}$ from 700 nm to 2900 nm in steps of 200 nm. The corresponding FWHM (see Table 1) was chosen to keep the number of optical cycles constant.

Table 1. The wavelength and corresponding pulse duration used in the calculations.

λ [nm]	700	900	1100	1300	1500	1700	1900	2100	2300	2500	2700	2900
FWHM [fs]	4.67	6.00	7.34	8.67	10.0	11.3	12.7	14.0	15.3	16.7	18.0	19.3

To describe the vibrational motions leading to deprotonation, we use the 2D basis |nm>, where |n0> is the IR-active anti-symmetric stretching mode (see Fig. 2(a)), |0m> the IR-inactive symmetric stretching mode (see Fig. 2(a)) and n, m the number of vibrational quanta. To simplify the following discussion we implicitly include the respective time evolution factor $e^{-i\left(\frac{E_{m,n}}{\hbar}\right)t}$.

The laser creates a wave packet $e^{-i\phi}|\,n0>$, where the phase ϕ of the vibrational wave packet matches the laser CEP φ. Because the light field can only address the IR-active modes |n0> the wave packet has no contribution of |0m>. If the laser is not resonant to the vibration this wave packet only forms temporarily and at the end of the laser pulse the |00> population is restored. Approaching the resonance frequency with the laser frequency in the MIR region increases the temporary population of |n0>. We assume in our simulations, that the molecule is ionized at the peak of the laser field. After around 3/4 of an optical cycle the released electron recollides with the parental cation, exciting the molecule to the reactive dication state $A^3\Pi_u$ (see Fig. 2(b)), where C-H/C-D bond cleavage occurs. Projection of the vibrational wave packets onto the corresponding ionic states is used to approximate the ionization steps.

The first ionization step is between the neutral molecule and the cationic molecule, where the first two electronic states ($X^2\Pi_u$ and $A^2\Pi_u$) are nearly degenerate. Therefore we project the neutral wave packet to both states with equal weight. For completeness the propagation in the cation included the possibility of population transfer between these two states, even if the effect is negligible as the transition dipole moment between those states along the investigated modes is extremely small.

The ionization leads to population of several cationic modes, including the IR-inactive ones |0m>, because the eigenfunctions of the molecular cation are slightly different from the ones of the neutral molecule so the projection of the |00> neutral mode is not the |00> cation mode. In contrast to the population of the IR-active modes, which is directly controlled by the laser and its CEP, this population process by ionization is independent of the CEP. The basic superposition of the fundamental IR-active and the IR-inactive modes,

$$\Psi_{basic} = |\,01> + e^{-i\phi}\,|\,10> \tag{3}$$

gives the important CEP-dependent part of the full wave packet.

The recolliding electron leads to the second ionization event. For this step the wave packet is projected onto the reactive, excited dicationic state $A^3\Pi_u$. Over a simulated time of 480 fs, with time steps of 0.24 fs, the wave packet is propagated on this PES and the part leaving the PES is used for calculating the deprotonation yield in the two directions.

The influence of Ψ_{basic} is illustrated in Fig. 3, where propagation of $\Psi_{basic}(0) = |\,01> + |\,10>$ and $\Psi_{basic}(\pi) = |\,01> - |\,10>$ for acetylene (white lines in Fig. 3) and deuterated acetylene (magenta lines in Fig. 3) on the reactive $A^3\Pi_u$ state shows a clear preference for the deprotonation direction. The principal mechanism is the same for both molecules, but for the deuterated molecules, the corresponding wave packet is slower and

Optics EXPRESS

more compact. While Ψ_{basic} helps to illustrate the underlying mechanism by concentrating on the |01> and |10> contributions all vibrational quanta are present in the calculations.

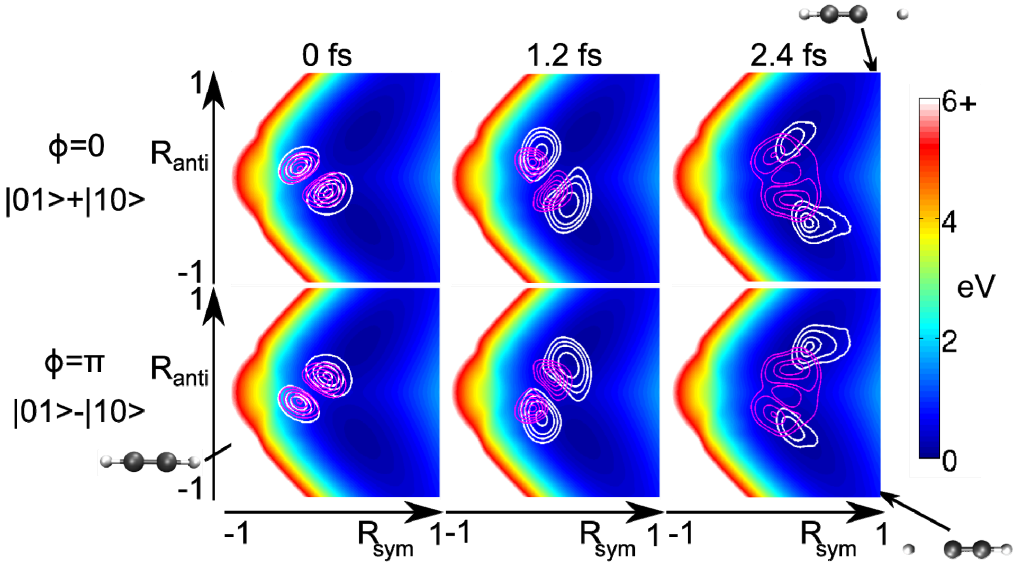

Fig. 3. Schematic of the control mechanism for deprotonation in acetylene. Vibrational wave packets of $\Psi_{basic}(0) = 01> +10>$ (top row) and the $\Psi_{basic}(\pi) = 01> -10>$ (bottom row) superposition (see text) are propagated on the PES of the first excited state of the acetylene dication along two normal modes. The contour lines display snapshots of the calculated nuclear wave packet which leads to deprotonation of the acetylene dication. The white contour lines correspond to acetylene and the magenta ones to deuterated acetylene. The CEP of the few-cycle pulse determines the sign in the superposition and thereby influences whether the right proton (top row) or the left proton (bottom row) dissociates.

4. Results and discussion

Dissociation of C-H bond is a fundamental and important process in hydrocarbon molecules, and is known to precede other reactions, such as reconstruction of chemical bonds and Coulomb explosion [42–44]. The attosecond control over the directionality of acetylene deprotonation has been demonstrated for few-cycle NIR laser fields [6, 14]. In our present work on the deprotonation of acetylene in few-cycle MIR laser fields, we measure the directionality of the H^+ ion emission from C_2H_2 and D^+ emission from C_2D_2. The momentum distributions of H^+/D^+ fragment ions as a function of CEP are recorded for an identical laser intensity of about 8×10^{13} W/cm^2. The obtained kinetic energy spectra for H^+/D^+ are shown in Fig. 4. The strong peaks centered around 5 eV for both H^+ and D^+ originate from deprotonation through the double ionization channel [45, 46]. The peak position for H^+ is at slightly higher kinetic energy compared to that for D^+ due to the difference in reduced masses. Beyond this peak, ion yields with higher kinetic energies, extending to about 20 eV, are observed for both molecules. A recent study utilizing NIR laser fields with pulse durations between 4.5 and 25 fs and intensities in the range 2-8 $\times 10^{14}$ W/cm^2, revealed that ions with such high kinetic energies originate from highly charged precursors of acetylene (with up to a 6 + charge state), in their case induced by multi-bond enhanced ionization [47]. For sufficiently long pulse durations the C-H bonds can stretch to their critical inter-nuclear distance for enhanced ionization [48, 49]. In our experiments the laser intensity is significantly smaller, however, the ponderomotive energy U_p is about 19 eV and the electron return energy can reach up to 3.17 U_p. Therefore, photoelectrons can recollide with an energy of up to around 60 eV, which appears sufficient for the population of the higher charge states

Optics EXPRESS

from which the multi-bond fragmentation of acetylene can take place and generate the observed high kinetic energy H^+ and D^+ fragments.

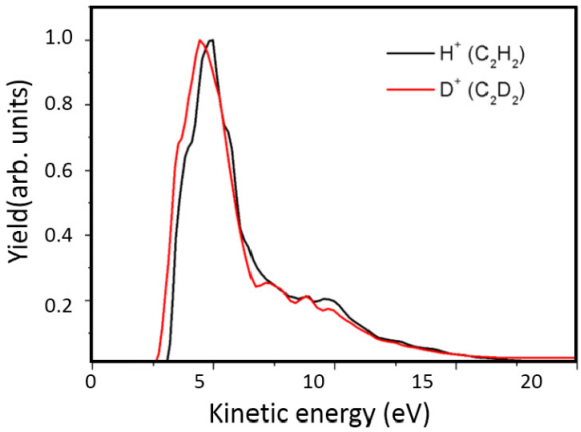

Fig. 4. The CEP-averaged kinetic energy spectra for H^+/D^+ from C_2H_2 /C_2D_2 obtained in linearly polarized few-cycle MIR laser fields at an intensity of about 8×10^{13} W/cm^2.

To quantitatively analyze the CEP-control of the directionality of the fragment ion emission, an asymmetry parameter is used which is defined as

$$A(\varphi, E) = \frac{Y_{up}(\varphi, E) - Y_{down}(\varphi, E)}{Y_{up}(\varphi, E) + Y_{down}(\varphi, E)}. \quad (4)$$

Here $Y_{up/down}(\varphi, E)$ represents the yield in the up/down part of the VMI images within a cone of 60 degrees half angle around the laser polarization. The CEP and ion energy are represented by the parameters φ and E, respectively. Since the number of images per CEP is not completely uniform, we have normalized the total ion yields for this analysis. Figure 5 presents the asymmetry parameter as a function of CEP and kinetic energy for both H^+ [Fig. 5(a)] and D^+ [Fig. 5(c)], with the kinetic-energy integrated asymmetry oscillations plotted in Figs. 5(b) and 5(d). Clear oscillatory behavior, with a period of 2π, is observed, for the kinetic energy region around 6-7 eV which we denoted as the low-KE region. No asymmetry oscillation is observed for high kinetic energies beyond 8 eV. For comparison, we plot the energy integrated asymmetry parameters for the kinetic energies near the cutoff (high-KE region). We can see in Figs. 5(b) and 5(d) that the asymmetry is almost zero for all the CEPs in the high-KE region, which can be expected for a multi-bond fragmentation mechanism, thus further supporting this assignment. The oscillation of the asymmetry as a function of CEP was fitted to the function $A(\varphi) = A_0 \cos(\varphi + \varphi_0)$, yielding the asymmetry amplitude A_0 and phase offset φ_0. As shown in Table 2, we determine an asymmetry amplitude for the low-KE region of about 1.0% for $H^+(C_2D_2)$ and 2.2% for $D^+(C_2D_2)$, respectively. The phase offsets of the asymmetry oscillations are rather similar in the experiments with 0.38 ± 0.05 rad for H^+ and 0.33 ± 0.04 rad for D^+. From a general point of view, we can conclude that the steering properties are similar for both $H^+(C_2H_2)$ and $D^+(C_2D_2)$, but the deuterated species shows stronger CEP-control. In our model the deciding contribution for the difference in asymmetry amplitude between acetylene and the deuterated acetylene is the projection of the neutral |00> (and |n0>) in cationic modes. Anomalous isotope effects have also been revealed for the electron-directed reactivity in the mid-infrared region which shown larger dissociation asymmetries for heavier isotopes [50].

Optics EXPRESS

Table 2. The amplitudes and phase offsets of asymmetry parameters for H^+/D^+ for the low-KE regions

	Amplitude A_0 (%)	Phase offset φ_0 (rad)
$H^+(C_2H_2)$	1.0 ± 0.1	0.38 ± 0.05
$D^+(C_2D_2)$	2.2 ± 0.1	0.33 ± 0.04

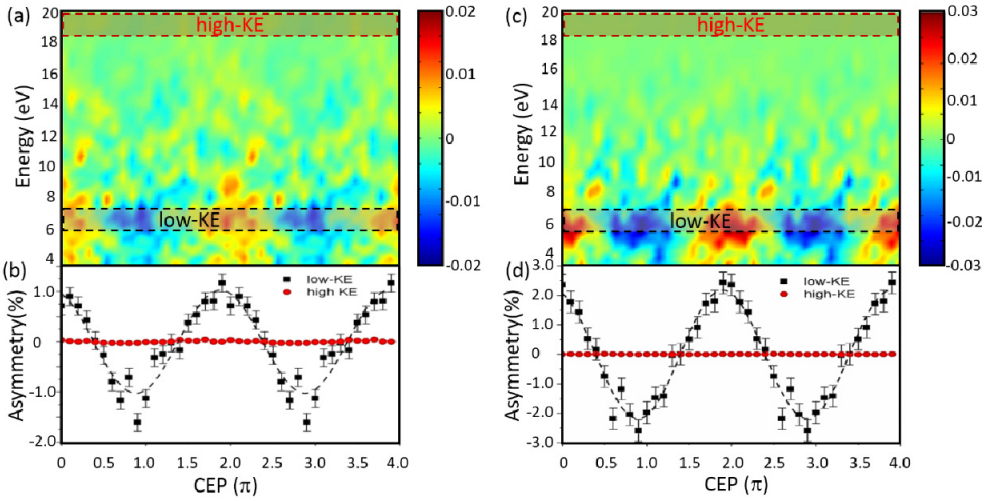

Fig. 5. The measured asymmetry parameter as a function of CEP and kinetic energy for (a) $H^+(C_2H_2)$ and (c) $D^+(C_2D_2)$. (b) and (d) show the kinetic energy integrated asymmetry oscillations for two KE regions. The dashed curves are the fitting results using a cosine function. Integration regions for the low- and high-KE are indicated by the areas enclosed by the black and red dashed rectangles, respectively.

Our quantum dynamical simulation is applied to C_2H_2 and C_2D_2 for the double ionization channel using the experimental laser parameters. The directionality of H^+/D^+ emission as a function of CEP is obtained for central wavelengths ranging from 700 nm to 2900 nm. The bandwidth for each central wavelength is chosen such that the Fourier transformed pulse duration has a constant number of optical cycles (see Tab 1.). The calculated amplitudes and phases for the asymmetry oscillations for the double ionization channel are plotted as a function of central wavelength in Fig. 6. The simulation results reveal a common tendency for the asymmetry amplitude for D^+ to be higher than that for H^+ for the double ionization channel in this spectral region, which agrees with our observations. However, there is discrepancy on the absolute value of the amplitude between experimental data and the calculated results. In the experiment, we get an amplitude of around 1.3-2.9%, while the amplitude from simulations can reach about 10% at 1.6 μm. A couple of issues can result in such discrepancy. For instance, the theoretical calculation is taken along the polarization axis while, due to limited signal-to-noise level, the experimental results are obtained from an integration over an angular range of ± 60 degrees along the polarization direction, which can result in a lower asymmetry parameter for the experimental results. Besides, the noise level in the experiment can reduce the asymmetry amplitude. On the other hand, the experimental results show that the phase offset is similar for H^+ and D^+ (listed in Table 2), which agrees fairly with the calculated results (shown in Fig. 6(b)). The calculated wavelength-dependent asymmetry parameters for the low-KE region provide us more insight on the steering of deprotonation process in MIR laser fields. From Fig. 6(a), we can see that, in general, the asymmetry parameter increases for longer wavelengths. This behavior can be attributed to a better match of the laser frequencies to the normal modes, especially the |10> mode, participating in the directional control. The much faster increase in the shorter wavelength regime and the dip around 2200 nm in the asymmetry parameter of C_2D_2 can be explained by

Optics EXPRESS

the changes in the vibrational wavefunctions induced due to deuteration. In C_2D_2, the optically addressable mode |20> is already populated in the first ionization step and the phase imprinted by the CEP of the light pulse can be opposed thereby diminishing the overall achieved asymmetry. The influence of the |20> mode can be also observed in the faster changing of the phase with wavelength for the deuterated acetylene.

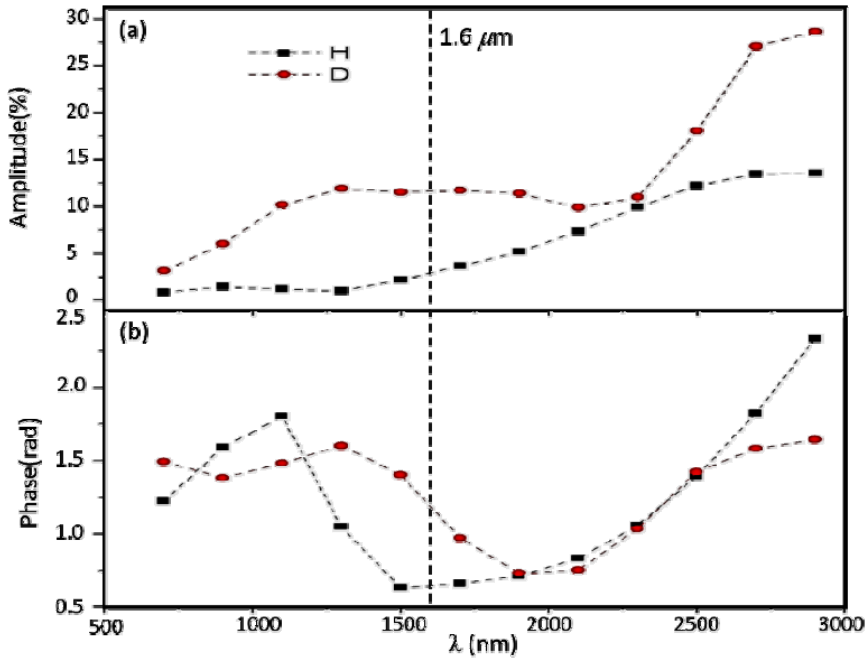

Fig. 6. The calculated (a) amplitudes and (b) phase offsets of the asymmetry parameters as a function of wavelength for H^+ (C_2H_2) and D^+(C_2D_2) at the intensity of 8×10^{13} W/cm^2. The asymmetry parameters are taken at their maximal value. A vertical dashed line marks the position of the central wavelength used in the experiment.

5. Conclusion

To summarize, we have investigated the directionality of the deprotonation of acetylene (C_2H_2) and the deuterated acetylene (C_2D_2) in waveform controlled few-cycle MIR laser pulses centered at 1.6 μm at an intensity of about 8×10^{13} W/cm^2. A dedicated stereo-ATI phase meter was developed for CEP-tagging experiments in the MIR and combined with VMI for studying the directional H^+/D^+ ion emission as a function of CEP. Clear asymmetry oscillations are observed for the deprotonation of C_2H_2 and C_2D_2. The asymmetry oscillation in the low-KE channel is assigned to deprotonation following double ionization, where asymmetry amplitudes of about 1.0% and 2.2% are obtained for H^+ and D^+, respectively. Our simulations are in fair agreement with the experimental results and they indicate a control of the directionality of deprotonation for longer wavelengths. The control mechanism is attributed to the superposition of normal modes induced by the intense laser fields, by which the reaction pathways can be steered via tuning the laser waveform with the CEP. We observed H^+ and D^+ fragments with high kinetic energies up to about 20 eV from the interaction of C_2H_2 and C_2D_2 with MIR few-cycle laser fields, which we attribute to highly charged precursors that undergo multi-bond fragmentation. Future studies using coincidence detection techniques could shine more light on the production of the high-energy ions in MIR laser fields. Based on the present results, which show an increased control over the

Optics EXPRESS

deprotonation of acetylene, we also expect a similar enhancement of the control of the isomerization of acetylene and other hydrocarbon molecules.

Funding

European Research Council (307203; 307270); Deutsche Forschungsgemeinschaft; King-Saud University; Max Planck Society; Natural Science Foundation of Shanghai (17YF1404000); National Natural Science Fund of China (NSFC) (11425416, 11374103, 61690224, and 11621404); Swiss National Science Foundation (200021_159875).

Acknowledgments

HL, CB, and MFK acknowledge support from the EU via the ERC grant ATTOCO (No. 307203). HL, NGK, CB, and MFK are grateful for support from the DFG via LMUexcellent. HL, NGK, CB, QL, MFK, RS, and RDVR acknowledge support from the DFG via the Munich Centre for Advanced Photonics. NGK, AMA, and MFK are also grateful for support from the King-Saud University in the framework of the MPQ-KSU-LMU collaboration (NGK, AMA, and MFK) and the visiting professorship program (MFK). JS acknowledges support from the Max Planck Society via the IMPRS-APS. HL is grateful for support from the Shanghai Sailing Program (Grant No. 17YF1404000). JW is grateful for the support from the National Natural Science Fund of China (11425416, 11374103, 61690224, and 11621404) and the 111 Project (B12024) of China. HJW acknowledges support from an ERC Starting Grant ATTOSCOPE (No. 307270) and the Swiss National Science Foundation through project no. 200021_159875.